2D Generalized Optical Spatial Modulation for MIMO-OWC Systems

Chen Chen, *Member, IEEE*, Lin Zeng, Xin Zhong, Shu Fu, Zhihong Zeng, Min Liu, and Harald Haas, *Fellow, IEEE*

***Abstract*—In this paper, a novel two-dimensional (2D) generalized optical spatial modulation (GOSM) scheme is proposed for multiple-input multiple-output optical wireless communication (MIMO-OWC) systems. By grouping multiple successive time slots as one time block, 2D GOSM mapping can be performed not only in the space domain but also in the time domain. Specifically, two types of 2D GOSM mapping schemes are designed, including 2D-1 and 2D-2 GOSM mappings. Moreover, to address the high complexity issue of optimal joint maximum-likelihood (ML) detection and the noise amplification and error propagation issues of zero-forcing-based ML (ZF-ML) detection, a deep neural network (DNN)-aided detection scheme is further designed for 2D GOSM systems. Simulation results demonstrate the superiority of the proposed 2D GOSM scheme with deep learning-aided detection for high-speed and low-complexity MIMO-OWC systems. More specifically, a remarkable 3.4-dB signal-to-noise ratio (SNR) gain can be achieved by 2D GOSM in comparison to the conventional one-dimensional (1D) GOSM, when applying the DNN-aided detection.**

***Index Terms*—Deep learning, multiple-input multiple-output, Optical wireless communication.**

I. Introduction

With the booming growth of mobile users in the coming years, the generated enormous data traffic will be far beyond the capacity of existing radio-frequency (RF) communication techniques. Thanks to its many inherent advantages such as abundant license-free spectrum and no electromagnetic interference radiation, optical wireless communication (OWC) has been envisioned as a promising complementary technology to alleviate the spectrum crunch [1]. In OWC systems using light-emitting diodes (LEDs) as optical transmitters, the available modulation bandwidth is usually small and hence the achievable capacity of OWC systems is greatly limited [2].

For a given modulation bandwidth, the capacity of OWC systems can be enhanced by improving the achievable spectral efficiency. To this end, various techniques have been reported to improve the spectral efficiency of bandlimited OWC systems recently. By fully exploiting the spatial domain resources, multiple-input multiple-output (MIMO) transmission has been widely shown as a promising technique for bandlimited OWC systems [3], [4]. Particularly, optical spatial modulation (OSM) has been attracting tremendous interest, due to its high power efficiency, negligible inter-channel interference and low implementation complexity [5], [6]. In order to improve the reliability of the overall OWC system, OSM has also been integrated with space time block codes (STBCs) [7]. However, it is challenging for OSM systems to achieve a high spectral efficiency, since only a single LED transmitter is activated for signal transmission at each time slot [8]. In order to enhance the spectral efficiency of OSM, generalized OSM (GOSM) schemes have been further proposed, which activate more than one LED to transmit the same constellation symbol at each time slot [9], [10]. Besides the spectral efficiency enhancement, GOSM can also provide spatial diversity to increase the signal-to-noise ratio (SNR) of the received constellation symbols. However, in all the existing GOSM systems, the GOSM mapping is one-dimensional (1D) which is generally performed only in the spatial domain.

In this paper, we for the first time propose and investigate a novel two-dimensional (2D) GOSM scheme for bandlimited MIMO-OWC systems. By grouping multiple successive time slots as one time block, GOSM mapping can be performed in both the spatial and time domains. Specifically, two types of 2D GOSM mapping schemes, i.e., 2D-1 and 2D-2 GOSM mappings, are designed within one time block. Moreover, three detection schemes, including joint maximum-likelihood (ML) detection, zero-forcing-based ML (ZF-ML) detection and deep neural network (DNN)-aided detection, are further proposed. It has been shown that the DNN-aided detection is able to mitigate the adverse effects of both noise amplification and error propagation suffered by the ZF-ML detection, while achieving near optimal performance as the joint ML detection with low computational complexity [10]–[13]. Numerical simulations are conducted to evaluate and compare the performance of the conventional 1D GOSM and the proposed 2D GOSM with different detection schemes.

Manuscript received 25 May 2022; revised 15 June 2022; accepted 18 July 2022. Date of publication 21 July 2022; date of current version 5 August 2022. This work was supported in part by the National Natural Science Foundation of China under Grant 61901065 and in part by the Natural Science Foundation of Chongqing under Grant cstc2021jcyj-msxmX0480. *(Corresponding author: Zhihong Zeng.)*

Chen Chen, Lin Zeng, Xin Zhong, Shu Fu, and Min Liu are with the School of Microelectronics and Communication Engineering, Chongqing University, Chongqing 400044, China (e-mail: c.chen@cqu.edu.cn; 202012021008@cqu.edu.cn; 201912131098@cqu.edu.cn; shufu@cqu.edu.cn; liumin@cqu.edu.cn).

Zhihong Zeng is with the LiFi Research and Development Centre, Institute for Digital Communications, The University of Edinburgh, EH9 3JL Edinburgh, U.K. (e-mail: zhihong.zeng@ed.ac.uk).

Harald Haas is with the Technology Innovation Centre and Department of Electronic and Electrical Engineering, University of Strathclyde, G1 1RD Glasgow, U.K. (e-mail: harald.haas@strath.ac.uk).

Digital Object Identifier 10.1109/JPHOT.2022.3192651

II. System Model

A typical MIMO-OWC system is considered here, which is equipped with N_t LEDs and N_r photo-detectors (PDs). Letting $\mathbf{s} = [s_1, s_2, \ldots, s_{N_t}]^T$ represent the transmitted signal vector, after transmission through the free-space channel, the received signal vector $\mathbf{y} = [y_1, y_2, \ldots, y_{N_r}]^T$ can be given by

$$\mathbf{y} = \mathbf{H}\mathbf{s} + \mathbf{n}, \tag{1}$$

where $\mathbf{H}$ and $\mathbf{n}$ denote the $N_r \times N_t$ MIMO channel matrix and the additive noise vector, respectively. Moreover, $\mathbf{H}$ can be expressed as follows:

$$\mathbf{H} = \begin{bmatrix} h_{11} & \cdots & h_{1N_t} \\ \vdots & \ddots & \vdots \\ h_{N_r1} & \cdots & h_{N_rN_t} \end{bmatrix}, \tag{2}$$

where h_{rt} is the direct current (DC) channel gain of the link between the t-th LED and the r-th PD, with $r = 1, 2, \ldots, N_r$ and $t = 1, 2, \ldots, N_t$. Without loss of generality, we assume that each LED follows the Lambertian radiation pattern here. Moreover, since the non-line-of-sight (non-LOS) components usually have a much lower electrical power than that of the LOS component during most channel conditions, it is generally reasonable to neglect the non-LOS components when calculating the DC channel gain [3]. Hence, we only take the LOS component into consideration and the corresponding LOS DC channel gain h_{rt} can be calculated by

$$h_{rt} = \frac{(l+1)\rho A}{2\pi d_{rt}^2}\cos^l(\varphi_{rt})T_s(\theta_{rt})g(\theta_{rt})\cos(\theta_{rt})\text{rect}\left(\frac{\theta_{rt}}{\Phi}\right), \tag{3}$$

where l is the Lambertian emission order and it is given by $l = -\ln 2/\ln(\cos(\Psi))$ with Ψ denoting the semi-angle at half power of the LED; ρ is the responsivity of the PD and A is the active area of the PD; d_{rt} is the transmission distance; φ_{rt} and θ_{rt} are the emission and the incident angles, respectively; $T_s(\theta_{rt})$ is the gain of optical filter, while $g(\theta_{rt}) = \frac{n^2}{\sin^2\Phi}$ is the gain of optical lens, with n and Φ being the corresponding refractive index and the half-angle field-of view (FOV), respectively; $\text{rect}(\frac{\theta_{rt}}{\Phi})$ is a rectangular function which indicates that the LOS DC channel gain is zero if the incident light is outside of the FOV of the receiver [14].

The additive noise in MIMO-OWC systems usually consists of shot noise, thermal noise and possibly excess noise. Generally, it is reasonable to model the additive noise as a real-valued zero-mean additive white Gaussian noise (AWGN) with a power of $P_n = N_0 B$, where N_0 is the noise power spectral density (PSD) and B is the signal bandwidth.

III. 2D GOSM for OWC

In this section, we first introduce the principle of 2D GOSM and then three spatial mapping schemes are described. Finally, three detection schemes for 2D GOSM are described.

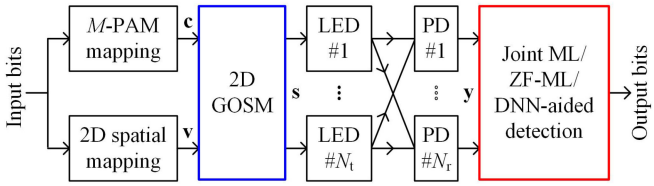

Fig. 1. Schematic diagram of the proposed 2D GOSM system.

A. Principle of 2D GOSM

Fig. 1 illustrates the schematic diagram of the proposed 2D GOSM system, where M-ary pulse amplitude modulation (M-PAM) is adopted. For M-PAM modulation, the intensity levels can be expressed as $I_m = \frac{2Im}{M+1}$ $(m = 1, \ldots, M)$, where I is the average emitted optical power. It can be seen that the input bits are first divided into two parts, i.e., the constellation part and the spatial part, which are then mapped into a PAM symbol vector $\mathbf{c}$ and a spatial index vector $\mathbf{v}$, respectively. Subsequently, 2D GOSM mapping is executed to generate the transmitted signal vector $\mathbf{s}$. At the receiver side, 2D GOSM detection, including the joint ML detection, the ZF-ML detection and the DNN-aided detection, is performed to yield the final output bits.

B. Three Spatial Mapping Schemes

In this subsection, three spatial mapping schemes are introduced, including conventional 1D spatial mapping and two novel 2D spatial mapping schemes, i.e., 2D-1 spatial mapping and 2D-2 spatial mapping. For conventional 1D spatial mapping, LED index selection is performed in each time slot independently. However, for the proposed 2D spatial mapping schemes, k successive time slots are grouped as one time block with $k \geq 2$ and LED index selection is jointly performed in the whole time block.

1) 1D Spatial Mapping: Fig. 2(a) shows the principle of conventional 1D spatial mapping, where N out of N_t LEDs are activated to transmit the same M-PAM symbol at each time slot, taking $N_t = 4$ and $N = 2$ for example. As a result, there are $C(N_t, N)$ possible LED activation patterns and $\lfloor \log_2 C(N_t, N) \rfloor$ spatial bits can be transmitted, where $C(\cdot, \cdot)$ denotes the binomial coefficient and $\lfloor \cdot \rfloor$ represents the floor operation. Hence, the spectral efficiency (bits/s/Hz) of 1D GOSM systems using M-PAM modulation is given by

$$R_{1\text{D}} = \log_2 M + \lfloor \log_2 C(N_t, N) \rfloor. \tag{4}$$

2) 2D-1 Spatial Mapping: In the proposed 2D-1 spatial mapping, k successive time slots are grouped as one time block to jointly perform LED index selection. More specifically, at the i-th $(i = 1, 2, \ldots, k)$ time slot in the time block, N out of N_t LEDs are activated to transmit the same M_i-PAM symbol. Fig. 2(b) depicts the principle of 2D-1 spatial mapping, where $N_t = 4$, $N = 2$ and $k = 2$. Taking the first time block τ_1 as an example, there are $C(N_t, N)$ possible LED activation patterns for both time slots t_1 and t_2. Hence, the total number of possible LED activation patterns over two time slots t_1 and t_2 within the time block τ_1 is given by $(C(N_t, N))^2$. Moreover, two different

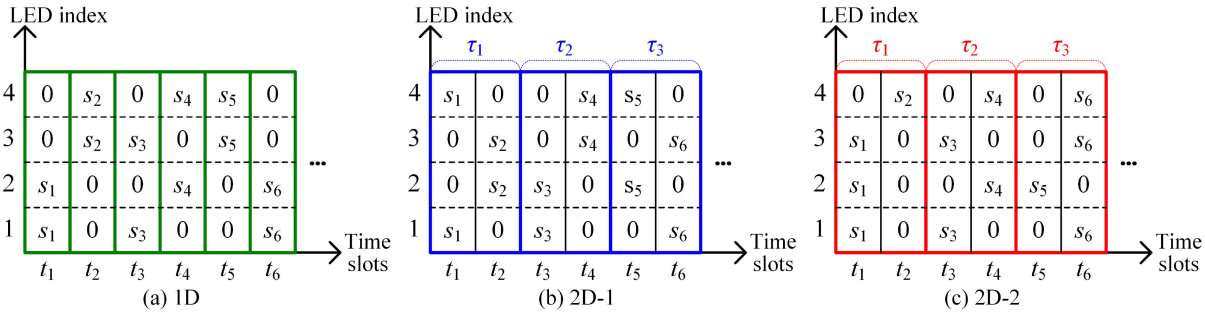

Fig. 2. Principle of (a) 1D GOSM, (b) 2D-1 GOSM and (c) 2D-2 GOSM, where $N_t = 4$, $N = 2$ and $k = 2$.

PAM symbols can be transmitted in the two time slots within one time block. Therefore, the spectral efficiency (bits/s/Hz) of 2D-1 GOSM systems with k successive time slots grouped in each time block is obtained by

$$R_{\text{2D-1},k} = \frac{1}{k}\sum_{i=1}^{k}\log_2(M_i) + \frac{1}{k}\lfloor k\log_2 C(N_t, N)\rfloor. \quad (5)$$

3) 2D-2 Spatial Mapping: Similarly, k successive time slots are also grouped as one time block to jointly perform LED index selection in the proposed 2D-2 spatial mapping. The principle of 2D-2 spatial mapping with $N_t = 4$, $N = 2$ and $k = 2$ is shown in Fig. 2(c). Differing from 2D-1 spatial mapping where N out of N_t LEDs are activated to transmit signal at each time slot, the number of activated LEDs in each time slot is not fixed in 2D-2 spatial mapping and only the total number of activated LEDs within each time block is fixed. Specifically, for each time block with k successive time slots, kN out of totally kN_t LEDs are activated to transmit signals and the number of activated LEDs at each time slot within the time block can be different. Thus, for 2D-2 spatial mapping, there are totally $C(kN_t, kN)$ possible LED activation patterns within one time block. Note that there should be at least one activated LED to transmit signal at each time slot within the time block, to ensure the successful transmission of constellation symbols. Consequently, the spectral efficiency (bits/s/Hz) of 2D-2 GOSM systems is given by

$$R_{\text{2D-2},k} = \frac{1}{k}\sum_{i=1}^{k}\log_2(M_i) + \frac{1}{k}\lfloor \log_2 C(kN_t, kN)\rfloor. \quad (6)$$

C. Three Detection Schemes for 2D GOSM

1) Joint ML Detection: Assuming perfect knowledge of the channel, joint ML detection is the optimal detection scheme for 2D GOSM systems using M-PAM modulation. Under joint ML detection, the transmitted signal vector $\mathbf{s}$ is estimated by

$$\hat{\mathbf{s}} = \arg\min_{\mathbf{s}\in\mathbb{S}} ||\mathbf{y} - \mathbf{H}\mathbf{s}||^2, \quad (7)$$

where $\mathbb{S}$ represents the set of all considered transmitted signal vectors and $\|\cdot\|$ denotes the Euclidean norm. Although joint ML detection can achieve optimal performance by evaluating the received signal vector $\mathbf{y}$ with respect to all the elements in $\mathbb{S}$ at each time, its computational complexity is relatively high and hence it might not be feasible in practical applications.

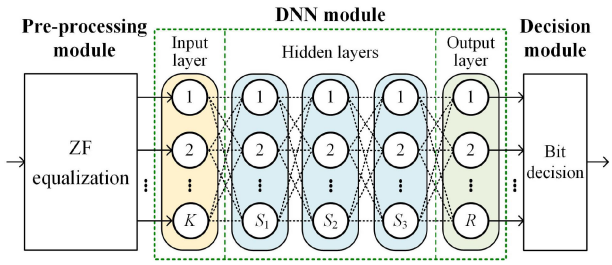

Fig. 3. Schematic diagram of the DNN-aided detection.

2) ZF-ML Detection: In comparison to the joint ML detection, ZF-ML detection achieves sub-optimal performance with much reduced computational complexity [11]. To apply ZF-ML detection in 2D GOSM systems, ZF equalization is first performed on the received signal vector $\mathbf{y}$ and thus the estimate of the transmitted signal vector $\mathbf{s}$ is expressed by

$$\hat{\mathbf{s}}_{\text{ZF}} = \mathbf{H}^{\dagger}\mathbf{y} = \mathbf{s} + \mathbf{H}^{\dagger}\mathbf{n}, \quad (8)$$

where $\mathbf{H}^{\dagger} = (\mathbf{H}^*\mathbf{H})^{-1}\mathbf{H}^*$ denotes the pseudo inverse of $\mathbf{H}$. After that, both the spatial index vector and the constellation symbol vector can be obtained from $\hat{\mathbf{s}}_{\text{ZF}}$ via conventional energy-based ML detection [4]. Despite its low computational complexity, ZF-ML detection suffers from the adverse effects of both noise amplification and error propagation.

3) DNN-Aided Detection: In order to simultaneously address the high complexity issue of joint ML detection and the noise amplification and error propagation issues of ZF-ML detection, a DNN-aided detection scheme is designed for 2D GOSM systems. Fig. 3 depicts the schematic diagram of the DNN-aided detection scheme, which consists of three key modules. The first one is the pre-processing module, which is used to perform ZF equalization on the received signal vector $\mathbf{y}$ so as to get the input vector of the DNN module. The second one is the DNN module, which contains one input layer, multiple hidden layers and one output layer. For the 2D GOSM systems with N_t LEDs, the input vector contains all the $2N_t$ symbols within one time block and hence the input layer contains $K = 2N_t$ neurons. Moreover, to efficiently learn the statistical characteristics of both the input signal and the additive noise, a total of three fully connected

TABLE I
SIMULATION PARAMETERS

Parameter	Value
Room dimension	4 m × 4 m × 3 m
LED spacing	2 m
APD spacing	15 cm
Semi-angle at half power of LED, Ψ	65°
Gain of optical filter, $T_s(\theta_{rt})$	0.9
Refractive index of optical lens, n	1.5
Half-angle FOV of optical lens, Φ	65°
Responsivity of APD, ρ	15 A/W
Height of receiving plane	1 m
Active area of APD, A	19.6 mm^2
Noise PSD, N_0	10^{-22}A^2/Hz
Modulation bandwidth, B	20 MHz
Number of LEDs, N_t	4
Number of activated LEDs, N	2
Number of APDs, N_r	4
Receiver location	(1.5 m, 1.5 m, 1 m)

hidden layers are adopted in the DNN module. The number of neurons in the l-th $(1 \leqslant l \leqslant 3)$ hidden layer is denoted by S_l and the rectified linear unit (ReLU) function is used as the activation function. Note that the number of hidden layers and the number of neurons adopted in each hidden layer are obtained after multiple trials, which can ensure that the DNN achieves satisfactory performance. For the output layer, it consists of R neurons, which is corresponding to the number of bits that can be transmitted during one time block, and the Sigmoid function is adopted as the activation function to obtain the output within the interval (0,1). Finally, the decision module estimates the final binary bits and the mean-squared error (MSE) loss function is exploited to measure the difference between the transmitted bit vector and the estimated bit vector. For more details about the DNN-aided detection, please refer to our previous work [10].

IV. SIMULATION RESULTS

In this section, simulations are performed to evaluate the performance of the proposed 2D GOSM systems using different detection schemes with different spectral efficiencies. We consider a 4×4 MIMO-OWC system in a typical 4 m × 4 m × 3 m room, where the 2 × 2 LED array is mounted at the center of the ceiling and the height of the receiving plane is 1 m. Moreover, avalanche PDs (APDs) are used in the system so as to enhance the SNR at the receiver side [4]. The key simulation parameters are listed in Table I. In order to accelerate the convergence speed, the mini-batch technique is employed in the training phase. The learning rate is 0.01 and Adamax is used as the optimizer. The parameters of the DNN-aided detectors for 1D, 2D-1 and 2D-2 GOSM systems are summarized in Table II. According to (4), (5) and (6), the required PAM orders of 1D, 2D-1 and 2D-2 GOSM systems to achieve target spectral efficiencies of 4 and 5 bits/s/Hz are given in Table III. In addition, due to the specific distance and emission/incident angle of each LED/PD pair in practical MIMO-OWC systems, the LOS DC channel gains of different LED/PD pairs might be different and hence the corresponding received SNRs might also be different. Instead, transmitted SNR, which is defined as the ratio of the transmitted electrical signal power P_s to the additive noise power P_n, can be adopted as a fair metric for bit error rate (BER) performance evaluation in practical MIMO-OWC systems [3], [4].

TABLE II
PARAMETERS OF DNN-AIDED DETECTORS

	Parameter	4 bits/s/Hz	5 bits/s/Hz
1D	Size of training set	200000	600000
	Number of neurons	20-24-20	120-128-120
	Size of mini-batch	100	200
2D-1	Size of training set	300000	400000
	Number of neurons	34-40-34	74-80-74
	Size of mini-batch	100	100
2D-2	Size of training set	400000	500000
	Number of neurons	60-64-60	120-128-120
	Size of mini-batch	200	200

TABLE III
PAM ORDER OF DIFFERENT SCHEMES

Scheme	4 bits/s/Hz	5 bits/s/Hz
1D	$M = 4$	$M = 8$
2D-1	$M_1 = 2$, $M_2 = 4$	$M_1 = 4$, $M_2 = 8$
2D-2	$M_1 = 2$, $M_2 = 2$	$M_1 = 4$, $M_2 = 4$

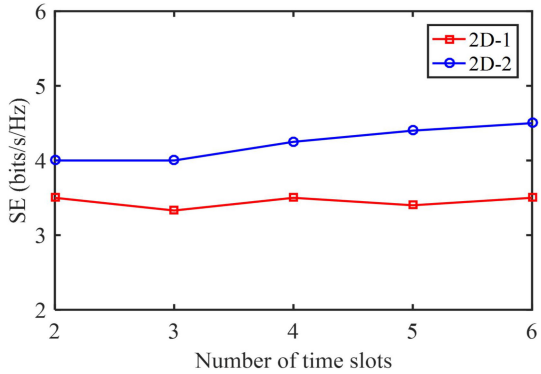

Fig. 4. Spectral efficiency vs. number of time slots k for 2D-1 and 2D-2 GOSM schemes with $N_t = 4$, $N = 2$ and $M_i = 2$ for $i = 1, 2, \ldots, k$.

A. Spectral Efficiency

Firstly, we analyze the relationship between the achievable spectral efficiency and the number of time slots within each time block for both 2D-1 and 2D-2 GOSM schemes. Fig. 4 shows the spectral efficiency versus the number of time slots k for 2D-1 and 2D-2 GOSM schemes with $N_t = 4$, $N = 2$ and $M_i = 2$ for $i = 1, 2, \ldots, k$. As we can see, when the number of time slots is increased, the spectral efficiency of 2D-1 GOSM is nearly stable at about 3.5 bits/s/Hz, while the spectral efficiency of 2D-2 GOSM is only slightly increased. More specifically, the spectral efficiency of 2D-1 GOSM for $k = 4$ is 3.5 bits/s/Hz, which is the same as that for $k = 2$. Moreover, the spectral efficiency of 2D-2 GOSM for $k = 4$ is 4.25 bits/s/Hz, which is only improved by 0.25 b/s/Hz in comparison to that for $k = 2$. Hence, the spectral efficiency of both 2D-1 and 2D-2 GOSM schemes cannot be

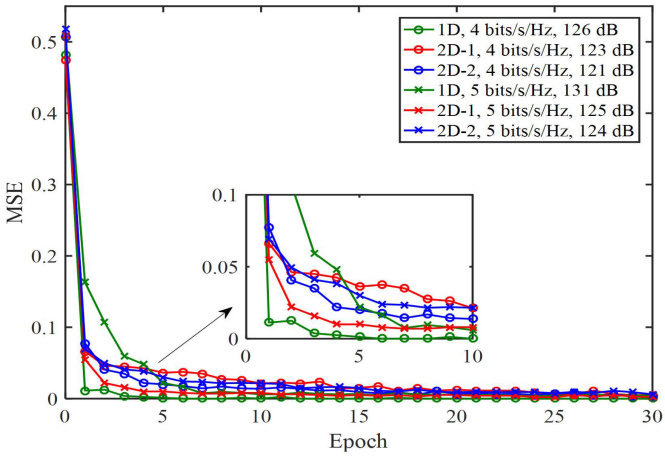

Fig. 5. MSE loss vs. epoch for the proposed DNN-aided detector.

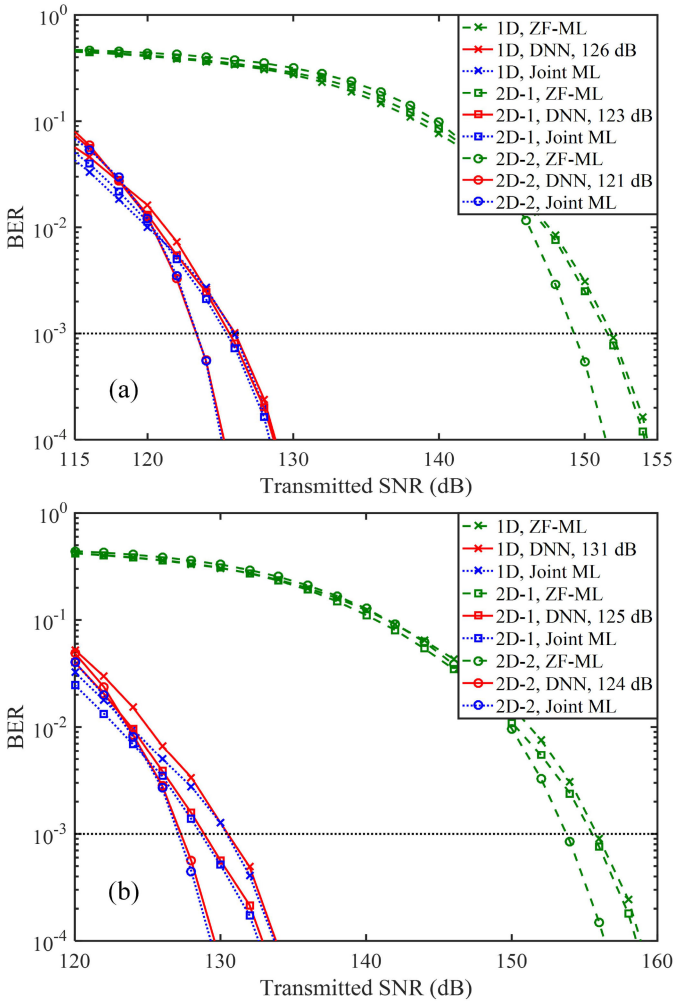

Fig. 6. BER vs. transmitted SNR for 1D, 2D-1 and 2D-2 GOSM systems with a spectral efficiency of (a) 4 bits/s/Hz and (b) 5 bits/s/Hz.

substantially improved by grouping more time slots within one time block. Furthermore, by grouping more time slots within one time block, the implementation complexity and the time delay are both inevitably increased. Therefore, it is feasible and appropriate to group only two time slots within one time block for both 2D-1 and 2D-2 GOSM schemes.

B. MSE Loss

Secondly, we evaluate the MSE loss of the DNN-aided detector. As shown in Fig. 5, the MSE drops rapidly for 1D, 2D-1 and 2D-2 GOSM systems when the number of epochs is slightly increased, and about 30 epochs are enough successfully train the DNN. Moreover, an appropriate transmitted SNR is selected to train the DNN for 1D, 2D-1 and 2D-2 GOSM systems with different spectral efficiencies, so as to ensure that the DNN can efficiently learn the statistical characteristics of both the input signal and the additive noise.

C. BER Performance

Thirdly, we investigate the BER performance of 1D, 2D-1 and 2D-2 GOSM systems with different detection schemes and spectral efficiencies. Figs. 6(a) and (b) compare the BER versus transmitted SNR with spectral efficiencies of 4 and 5 bits/s/Hz, respectively. For a spectral efficiency of 4 bits/s/Hz as shown in Fig. 6(a), when using ZF-ML detection, 2D-1 GOSM performs slightly better than 1D GOSM while 2D-2 GOSM outperforms 2D-1 GOSM by an SNR gain of 2.2 dB. In contrast, when the DNN-aided detection with optimal training SNRs is applied, all the three GOSM systems obtain nearly the same BER performance as that applying joint ML detection. More specifically, the required SNRs to reach BER $= 10^{-3}$ are 126, 125.4 and 123.4 dB for 1D, 2D-1 and 2D-2 GOSM systems, respectively. Hence, a significant SNR gain of 26 dB is achieved for all three GOSM systems compared with that using the ZF-ML detection. Similarly, 1D and 2D-1 GOSM systems achieve comparable BER performance, while 2D-2 GOSM obtains an SNR gain of 2.6 dB in comparison to 2D-1 GOSM at BER $= 10^{-3}$. For a higher spectral efficiency of 5 bits/s/Hz as shown in Fig. 6(b), 2D-1 GOSM still slightly outperforms 1D GOSM with ZF-ML detection. However, 2D-1 GOSM achieves an SNR gain of 1.7 dB over 1D GOSM when applying DNN-aided detection. In addition, a remarkable SNR gain of 3.4 dB is achieved by 2D-2 GOSM in comparison to 1D GOSM. It can be clearly observed from Figs. 6(a) and (b) that 2D-2 GOSM with the DNN-aided detection achieves the best BER performance among all the considered schemes.

D. Computational Complexity

Finally, we compare the computational complexity of three detection schemes in terms of computation time. The computation was performed using JetBrains PyCharm with an AMD Ryzen 5 3600 CPU, 16 GB RAM, and NVIDIA GeForce GTX 1660 SUPER GPU. Considering that the training of DNN can be performed offline in advance, it is reasonable to only take the online detecting phase into account when evaluating the computational complexity of the DNN-aided detection scheme [10],

TABLE IV
COMPARISON OF COMPUTATION TIME

Scheme		4 bits/s/Hz	5 bits/s/Hz
1D	Joint ML	4.61 s	7.31 s
	ZF-ML	1.31 s	1.51 s
	DNN	1.25 s	1.50 s
2D-1	Joint ML	4.03 s	6.13 s
	ZF-ML	1.77 s	1.95 s
	DNN	1.39 s	1.66 s
2D-2	Joint ML	7.04 s	10.51 s
	ZF-ML	2.78 s	2.94 s
	DNN	1.63 s	1.81 s

[11]. Table IV compares the computation time of three detection schemes with two spectral efficiencies of 4 and 5 bits/s/Hz. For the 1D GOSM system with a spectral efficiency of 4 bits/s/Hz, the computation time of the DNN-aided detector is comparable as that of the ZF-ML detector, which is much shorter than that of the joint ML detector. For the 2D-1 and 2D-2 GOSM systems with a spectral efficiency of 4 bits/s/Hz, the computation time of the DNN-aided detector becomes shorter than that of the ZF-ML detector. The same conclusion can also be found for 1D, 2D-1 and 2D-2 GOSM systems with a spectral efficiency of 5 bits/s/Hz. Therefore, the proposed DNN-aided detector is shown to be a low-complexity detector that can achieve near-optimal BER performance.

V. CONCLUSION

In this paper, we have proposed a novel 2D GOSM scheme with deep learning-aided detection for MIMO-OWC systems. Compared with conventional 1D GOSM mapping, the proposed two 2D GOSM mapping schemes, namely 2D-1 and 2D-2 GOSM mappings, can achieve higher spectral efficiencies. Moreover, the proposed DNN-aided detection obtains comparable BER performance as the optimal joint ML detection, but with much reduced computational complexity. Our simulation results show that 2D-2 GOSM with DNN-aided detection achieves the best BER performance for two target spectral efficiencies. Therefore, the proposed deep learning-aided 2D GOSM scheme can be a promising candidate for high-speed and low-complexity MIMO-OWC systems.

REFERENCES

[1] T. Cogalan and H. Haas, "Why would 5G need optical wireless communications?," in *Proc. IEEE Annu. Int. Symp. Pers., Indoor Mobile Radio Commun.*, 2017, pp. 1–6.

[2] S. Rajagopal, R. D. Roberts, and S.-K. Lim, "IEEE 802.15. 7 visible light communication: Modulation schemes and dimming support," *IEEE Commun. Mag.*, vol. 50, no. 3, pp. 72–82, Mar. 2012.

[3] T. Fath and H. Haas, "Performance comparison of MIMO techniques for optical wireless communications in indoor environments," *IEEE Trans. Commun.*, vol. 61, no. 2, pp. 733–742, Feb. 2013.

[4] C. Chen et al., "OFDM-based generalized optical MIMO," *J. Lightw. Technol.*, vol. 39, no. 19, pp. 6063–6075, Oct. 2021.

[5] R. Mesleh, H. Elgala, and H. Haas, "Optical spatial modulation," *J. Opt. Commun. Netw.*, vol. 3, no. 3, pp. 234–244, Mar. 2011.

[6] M. D. Soltani et al., "Bidirectional optical spatial modulation for mobile users: Toward a practical design for LiFi systems," *IEEE J. Sel. Areas Commun.*, vol. 37, no. 9, pp. 2069–2086, Sep. 2019.

[7] S. Naser, L. Bariah, S. Muhaidat, M. Al-Qutayri, M. Uysal, and P. C. Sofotasios, "Space-time block coded spatial modulation for indoor visible light communications," *IEEE Photon. J.*, vol. 14, no. 1, Feb. 2022, Art. no. 7303111.

[8] X. Zhu, Z. Wang, Q. Wang, and H. Haas, "Virtual spatial modulation for MIMO systems," in *Proc. IEEE Glob. Commun. Conf.*, 2016, pp. 1–6.

[9] C. R. Kumar and R. Jeyachitra, "Power efficient generalized spatial modulation MIMO for indoor visible light communications," *IEEE Photon. Technol. Lett.*, vol. 29, no. 11, pp. 921–924, Jun. 2017.

[10] C. Chen, L. Zeng, X. Zhong, S. Fu, M. Liu, and P. Du, "Deep learning-aided OFDM-based generalized optical quadrature spatial modulation," *IEEE Photon. J.*, vol. 14, no. 1, Feb. 2022, Art. no. 7302306.

[11] T. Wang, F. Yang, and J. Song, "Deep learning-based detection scheme for visible light communication with generalized spatial modulation," *Opt. Exp.*, vol. 28, no. 14, pp. 21202–21209, Sep. 2020.

[12] X. Zhong et al., "Joint detection for generalized optical MIMO: A deep learning approach," in *Proc. IEEE Conf. Ind. Electron. Appl.*, 2021, pp. 1317–1321.

[13] X. Zhong, C. Chen, S. Fu, Z. Zeng, and M. Liu, "DeepGOMIMO: Deep learning-aided generalized optical MIMO with CSI-free blind detection," 2021. [Online]. Available: https://arxiv.org/abs/2110.04084

[14] P. H. Pathak, X. Feng, P. Hu, and P. Mohapatra, "Visible light communication, networking, and sensing: A survey, potential and challenges," *IEEE Commun. Surv. Tut.*, vol. 17, no. 4, pp. 2047–2077, Oct.–Dec. 2015.